such that after the first stage they have the right quantity to yield a sufficiently homogeneous particle of 3:1 composition. This process provides the continuous pathway for shielding currents. At the other extreme of nominal composition, the smaller grains become superconducting during the diffusion stage, but upon homogenization this superconductivity is destroyed by the excess K, much as the normal state conductivity is destroyed by extended doping (*5*), as supported by photoemission results (*10*) and orbital-filling arguments (*5*). On the other hand, the larger than average grains, at equilibrium, can turn out to have the right concentration to be superconducting. This accounts for the nearly symmetrical curve of shielding diamagnetism curve versus nominal composition (Fig. 2) and also for the rise and fall of shielding diamagnetism as a function of heat treatment in the high-x samples. The sample with the observed maximum shielding diamagnetism corresponds to transforming to the right concentration the average grain size and hence the majority of grains. We believe this conclusion reflects the inherent limitations of the gas-solid reaction procedure. Different techniques, such as precipitation from organic solution, could result in higher yields. This is why we view the >40% value as a very high yield from these powder samples.

The actual quality of the material obtained here has provided the capability to measure critical field curves $H_{c1}(T)$ and $H_{c2}(T)$ (*9*). The zero-temperature extrapolated values are $H_{c1}=132$ G and $H_{c2}=49$ T. These values allow one to evaluate the penetration depth $\lambda = 2400$ Å and the coherence length $\xi = 26$ Å, and hence a Ginzburg-Landau parameter $\kappa = \lambda/\xi$ around 100, an extremely high value approaching that of the high-T_c copper oxides.

We find that it is the K_3C_{60} composition that is the superconducting phase, and neither under- nor overdoped phases (relative to the correct one) are superconducting. The discovery of the $T_c = 30$ K superconducting phase of Rb_xC_{60} should stringently test the different theoretical possibilities, as it offers the possibility of comparing the dependence of T_c on slight chemical modifications. Prerequisite to this is a completion of the systematic study of the phase diagram of Rb and other alkali-C_{60} mixtures.

Note added in proof: During these studies we learned that Rosseinsky *et al.* (*11*) found a superconducting transition at 28 K in a Rb-doped C_{60} sample.

REFERENCES AND NOTES

1. W. Krätschmer, L. D. Lamb, K. Fostiropoulos, D. R. Huffman, *Nature* **347**, 354 (1990).
2. H. Aije *et al.*, *J. Phys. Chem.* **94**, 8630 (1990).
3. R. Taylor, J. P. Hare, A. K. Abdul-Sada, H. W. Kroto, *J. Chem. Soc. Chem. Commun.* **1990**, 1423 (1990).
4. P.-M. Allemand *et al.*, *J. Am. Chem. Soc.* **113**, 2780 (1991).
5. R. C. Haddon *et al.*, *Nature* **350**, 320 (1991).
6. A. F. Hebard *et al.*, *ibid.*, 600.
7. M. Tinkham, *Introduction to Superconductivity* (McGraw-Hill, New York, 1975).
8. K. Holczer *et al.*, unpublished results.
9. K. Holczer *et al.*, unpublished results.
10. P. J. Benning, J. L. Martins, J. H. Weaver, L. P. F. Chibante, R. E. Smalley, *Science*, in press.
11. M. J. Rosseinsky *et al.*, *Phys. Rev. Lett.*, in press.

12. S. J. Anz and F. Ettl produced and separated the molecular carbon samples used in this research. Supported by NSF grants (to R.L.W. and F.N.D. and to R.B.K.) and by the David and Lucille Packard Foundation (R.L.W. and R.B.K.).

8 May 1991; accepted 10 May 1991

New Mechanism of Cavitation Damage

YOU LUNG CHEN AND JACOB ISRAELACHVILI

Enormous impact pressures can develop when a vapor cavity collapses in a liquid, and it is generally held that these pressures are the underlying cause of cavitation damage of surfaces. The rapid growth and disappearance of vapor cavities have been viewed with a surface forces apparatus in liquids, and their effects on nearby surfaces at the submicroscopic level have been simultaneously monitored. The inception of cavities is intimately connected with simultaneous relaxations of high local strain energies on nearby surfaces, and in many practical situations, damage is more likely to occur during the formation, rather than the collapse, of cavities.

CAVITATION DAMAGE OF SURFACES in liquids is an important industrial and biological problem, for example, in the damage or erosion of propeller blades, high-speed lubricated bearings, and metal surfaces subjected to ultrasonic vibrations, in the wear of knee joints, and in decompression sickness (the bends). On the basis of Rayleigh's classic 1917 paper on collapsing bubbles (*1*), cavitation damage was thought to be due solely to the extremely large implosive pressure generated at the moment when a vacuum cavity or bubble collapses. During the 1960s, it was shown that bubbles deform during collapse and that damage is also caused by the impacts of high-speed liquid jets that strike surfaces during the collapse phase, producing tiny pits or craters on the surfaces (*2*). The evidence that most directly links surface damage to bubble collapse has come from experiments with hydrofoils in cavitation tunnels, which generally show that maximum erosion along a hydrofoil surface usually correlates well with the location of collapsing bubbles (*3*).

Less direct but more detailed information has been gained from laboratory experiments in which high-voltage electric sparks or pulsed laser beams are used to artificially nucleate bubbles at specific locations within a liquid near a surface. Their subsequent time evolution is then recorded with a high-speed camera (*4, 5*). Such experiments have so far not been able to determine the exact stage of the inception-growth-collapse cycle of bubbles at which damage occurs (*6*). The whole process of cavity growth and collapse usually occurs very rapidly (10^{-6} to 10^{-3} s), and all of the interesting features have submicroscopic dimensions. For these reasons, it has been difficult to study the rapid growth and collapse of cavities and especially the relation of these processes to the (elastohydrodynamic) surface deformations and, ultimately, damage. However, it is generally believed that damage occurs only during the collapse (*4–7*).

The subject has received much theoretical attention, but it has proved too difficult to arrive at a general theory that satisfactorily accounts, even qualitatively, for many of the observed phenomena (*6, 8*). Most theoretical treatments start with cavities or gas bubbles already present in the liquid and then attempt to determine the course and consequence of their collapse. Curiously, little theoretical or experimental attention has been given to bubble formation under natural conditions and the effects of the first shock wave produced by rapidly growing bubbles (*6*).

Using the surface forces apparatus (SFA) technique (*9*) in studies of elastohydrodynamic deformations of two curved surfaces moving toward or away from each other in liquids, we noticed that vapor cavities developed when the surfaces were separated faster than some critical velocity. Because the optical technique used in these measurements (*10*) enables one to follow surface deformations in real time (*11, 12*) and to observe vapor cavities form (*13*) at the nanometer level, we decided to study the phenomenon of cavity formation and collapse in detail.

The SFA, with its molecularly smooth

Department of Chemical and Nuclear Engineering and Materials Department, University of California, Santa Barbara, CA 93106.

surfaces and angstrom resolution capability, has been used mostly to measure the forces between surfaces in liquids. The optical interference technique, which uses "fringes of equal chromatic order" (FECO), allows one to measure not only the distance between the two surfaces at any point (*10, 12*) but also their changing shape with time (*11*) and the evolution of liquid bridges (*14*) or cavities (*13*) between the surfaces. Thus, one can identify when and where cavitation damage occurs and how it spreads in model systems. We have found that all of these processes can be slowed (which makes detailed video recordings (*11*) of these events possible) by using liquids of very high viscosities.

A conventional SFA was used with two video cameras. One camera was used as a normal optical microscope for directly viewing the surfaces; the other monitored the moving FECO fringes. The former provided a top view of the two apposing surfaces and of the cavities between them, and the latter provided angstrom-scale resolution of surface profiles and refractive index discontinuities in the liquid (*10, 13, 14*). We used low molecular weight polymer liquids of polybutadiene (PBD) with molecular weight in the range 4×10^3 to 10×10^3 and viscosities in the range 10 to 180 poise (P) (*15*).

The two surfaces were arranged to face each other in a crossed cylinder configuration. Because the radius R of each surface (~1 cm) is much greater than the separation D, this geometry is similar to a sphere near a flat surface or to two spheres close together. A large droplet of liquid was injected between the two curved surfaces, and the atmosphere inside the chamber was controlled so that the gases dissolved in the liquids were atmospheric air, dry nitrogen, or water. The molecularly smooth surfaces were either bare mica (a high-energy polar surface having strong adhesion to the liquid) or surfactant-coated mica (a low-energy inert hydrocarbon surface having weak adhesion to the liquid). The following qualitative features of the approach and separation of two surfaces were found to be the same for all of the liquids and surfaces studied.

Two initially curved, elastic mica surfaces were made to approach each other at various initial driving velocities v between 0.01 and 5 μm/s. Elastohydrodynamic flattening of the surfaces was observed to start at some finite surface separation of 10 to 200 nm. The flattening occurs as a result of the increasing viscous forces that elastically compress the material (glue layer and glass disks) supporting the thin mica sheets. The surface separation at which flattening begins depends on the elastic modulus of the underlying material, on the velocity of approach, and on the viscosity of the liquid.

Figure 1 shows the FECO fringe pattern changing with time for two approaching surfaces in PBD with a viscosity of 180 P. Initially (Fig. 1A) the surfaces approach each other at a steady velocity v but do not deform. When the surfaces are ~50 nm apart (Fig. 1B), they begin to slow down relative to each other as a result of the flattening and compression of the supporting material. From Fig. 1B to Fig. 1C the surfaces bulge inward; that is, they become "bell-shaped"—a characteristic feature of elastohydrodynamic deformations of two approaching surfaces (*16*). In Fig. 1C the driving velocity was reduced to zero, so that from Fig. 1C to Fig. 1D the surfaces relax naturally to equilibrium. The surfaces equilibrate in a flattened configuration at a separation of D = 13 nm; this value is determined by the short-range repulsive force between the two surfaces across the liquid film (*17*).

The reverse process of separating two surfaces after they have been brought together is shown in Figs. 2 and 3. The surfaces do not return to their original curved shapes simply by reversing the path taken on approach; this phenomenon does not appear to have been much studied nor is its importance fully appreciated (*16*). In addition, when two surfaces are separated in liquid, two different paths can be taken depending on the speed of the separation: the first does not involve the formation of cavities, and the second does.

At low speeds (v < 0.05 μm/s), the separation is "continuous" or "smooth," as shown in Fig. 2, A through F, and Fig. 3, top. During separation the initially flattened mica surfaces go through a stage in which they become pointed; that is, they bulge outward. As they move apart, their shape becomes less pointed and eventually returns to the original undeformed shape.

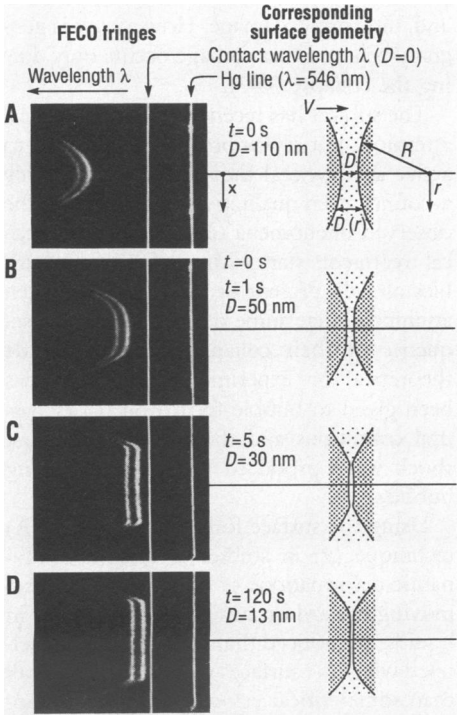

Fig. 1. Changing FECO fringe pattern with time t [(**A**) 0 s; (**B**), 1 s; (**C**), 5 s; and (**D**), 120 s] as two curved surfaces with initial (undeformed) radius of $R \approx 1$ cm approach each other in liquid polybutadiene (PBD) at a velocity v of 0.1 μm/s. The surface profile $\lambda(x)$ in the spectrogram (left) gives the separation profile $D(r)$ of the two surfaces (right) (*10–12*).

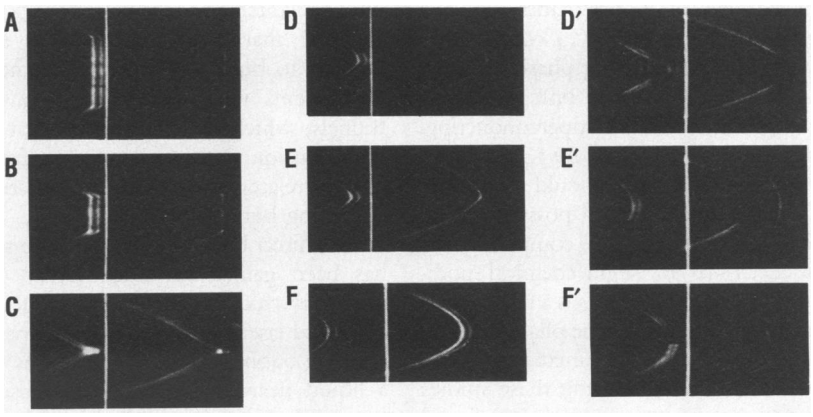

Fig. 2. Changing FECO fringe pattern with time t during the separation of two surfaces in a high-viscosity liquid starting at (**A**) t = 0, displacement D = 13 nm, from flattened contact (as in Fig. 1D). (**B**) t = 6 s, D = 14 nm. (**C**) t = 10.48 s, D = 16 nm. At low separation velocities the surfaces separate without evidence of cavitation: (**D**) t = 21 s, D = 36 nm; (**E**) t = 50 s, D = 50 nm; and (**F**) t = 100 s, D = 110 nm. At separation velocities slightly greater than v_c, a vapor cavity forms at the center, seen here as a discontinuity in the fringe pattern at (**D′**) t = 10.50 s, D = 44 nm. The cavity persists for several seconds: (**E′**) t = 17 s, D = 250 nm; and (**F′**) t = 22 s, D = 1000 nm. The corresponding shapes of the surfaces are shown schematically in Fig. 3 (top) for (A) through (F) and in Fig. 3 (middle) for (A) through (F′).

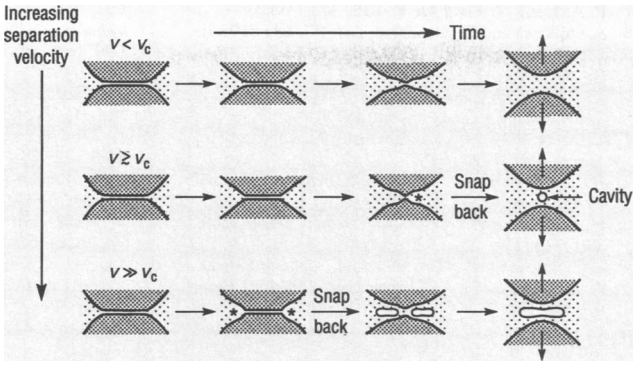

Fig. 3. Schematic illustration of the separation of two curved mica surfaces at progressively increasing separation velocities as ascertained from the FECO fringe pattern (Fig. 2) and direct optical microscope visualization (*19, 20*). The most likely places where recoil and damage occurred are shown by the starred points (*). (**Top**) $v < v_c$: smooth separation; no cavities. (**Middle**) $v \geq v_c$: abrupt separation; cavity and damage form at center. (**Bottom**) $v \gg v_c$: abrupt separation; cavities and damage form at rim (crater-like).

If the speed of separation is increased, the surfaces become more pointed, that is, elastically more strained, just before they rapidly move apart. This behavior indicates that the largest stresses on both the surfaces and liquid occur at this highly pointed central region. Then, above some critical speed v_c (here ~1 μm/s), a completely new separation mechanism takes over, shown in Fig. 2, A through F′, and Fig. 3, middle. Instead of separating smoothly, the liquid "fractures" or "cracks" open like a solid (*18*). This process releases the high tensile stress and allows the pointed surfaces to suddenly snap back to their original rounded shape and, simultaneously, allows a vapor cavity to grow between the two recoiling surfaces. This process is shown in Fig. 2D′, in which a 44-nm-thick cavity has formed. The recoil is so rapid (instantaneous on our 0.02-s resolution video recording) that the impact pressures developed must be extremely large. Judging from the much slower (on a time scale of seconds) and gentler surface deformations associated with the subsequent collapse of the cavities, we conclude that the initial "recoil pressure" must be much larger than the bubble collapse or jet impact pressure (at least in this system).

Qualitatively, the whole "recoil process" may be considered analogous to pulling a mass away from a surface to which it is attached by a spring, and then—when the spring is taut—suddenly letting go. As the mass strikes and then rebounds from the surface, enormous pressures (first tensile, then compressive, then tensile again on the rebound) will be felt, both by the mass and the surface. Whenever irreversible surface damage occurred in this system, it occurred only during surface recoil.

When the speed of separating two surfaces is increased to well above v_c, cavitation occurs even before the elastically deforming surfaces have reached the pointed stage. Under these conditions, cavitation occurs on a circle around the center where the two surfaces sharply bifurcate (Figs. 2B and 3, bottom). At the instant of cavitation, the surface geometry is like that of two circular craters, one turned over the other, and the rims of the craters snap back, leaving behind a doughnut-shaped cavity. This cavity then coalesces into a single disk-like cavity or bubble that proceeds to collapse by "fingering" inward. Time-lapse optical microscope photographs of these collapsing cavities (*19*) show that during the collapse a cavity goes through a rosette shape similar to a photograph of Dowson and Taylor (*20*).

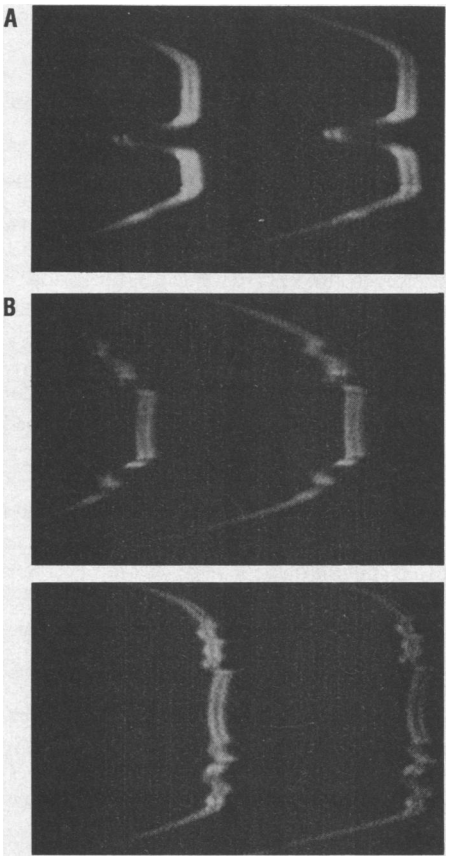

Fig. 4. Erosion damage, seen as irregular ripples on otherwise smooth FECO fringes, occurs at the center of the contact zone when $v \geq v_c$ (**A**) and on a circular rim around the center when $v \gg v_c$ (**B**); these cases correspond to the middle and bottom rows of Fig. 3, respectively.

The process just described indicates that at sufficiently high separation speeds, two contacting surfaces do not have enough time to elastically relax from their initially curved or flattened state—even if they are not in contact but are separated by a very thin film of liquid. Maximum negative pressure is thus reached at some finite radial distance from the center, and it is here that the surfaces snap back (recoil), cavities form (but do not necessarily collapse), and damage occurs.

We have found that cavitation bubbles can occur either totally within the liquid, that is, away from the surfaces, or at the solid-liquid interfaces. The adhesion of untreated (polar) mica surfaces to the PBD liquid is stronger than the cohesion between the liquid molecules themselves ("wetting" conditions); hence, the cavities form totally within the liquid. In contrast, for surfaces coated with a surfactant monolayer, the nonpolar solid-liquid adhesion is weaker (*21*), and the cavities form at the interfaces.

We conclude that damage generally occurs only during the formation of cavities, when the surfaces recoil, but neither during the collapse of cavities nor at the place of collapse. This conclusion was reached in two ways: (i) At high separation velocities, cavities occurred at the center of the contact zone, and the surfaces could be brought back together again before the bubbles had disappeared (collapsed). From the deformed shapes of the FECO fringes (Fig. 4A), one could discern that two initially undamaged surfaces were already damaged at the center. The bubbles usually moved to another place before disappearing without causing any discernible damage there. (ii) At even higher separation speeds, cavities formed in a ring around the contact region, and damage occurred in this region (Fig. 4B). It is likely that a similar damage mechanism occurs in systems in which cavities are produced near a moving surface or between two moving surfaces, for example, between roller bearings and during the lubricated sliding of two surfaces. The idea that damage can occur during surface recoil also readily accounts for how material can be removed from a solid surface ("erosion" damage).

Our findings suggest that to better understand how to avoid cavitation damage, researchers need to conduct new types of experiments in which more attention is given to the elastohydrodynamic deformations of surfaces before and during cavity formation and also to the material and wettability properties of surfaces, which determine where bubble inception and growth is most likely to occur.

REFERENCES AND NOTES

1. Lord Rayleigh, *Philos. Mag.* **34**, 94 (1917).
2. T. B. Benjamin and A. T. Ellis, *Philos. Trans. R. Soc.*

London Ser. A **260**, 221 (1966).
3. R. T. Knapp, J. W. Daily, F. G. Hammitt, in *Cavitation* (McGraw-Hill, New York, 1970), chap. 8; J. H. J. Van der Meulen and Y. Nakashima, in *Cavitation*, S. P. Hutton, Ed. (Mechanical Engineering Publications, London, 1983), pp. 13–19; R. Simoneau, F. Avellan, Y. Kuhn de Chizelle, in *International Symposium on Cavitation Noise and Erosion in Fluid Systems*, R. E. A. Arndt, Ed. (American Society of Mechanical Engineers, New York, 1989), vol. 88, pp. 95–102.
4. J. R. Blake and D. C. Gibson, *Annu. Rev. Fluid Mech.* **19**, 99 (1987).
5. D. H. Trevena, *Cavitation and Tension in Liquids* (Hilger, Bristol, 1987), chaps. 6 and 8.
6. A. Vogel, W. Lauterborn, R. Timm, *J. Fluid Mech.* **206**, 299 (1989); Y. Tomita and A. Shima, *ibid.* **169**, 535 (1986).
7. P. A. Lush, *J. Fluid Mech.* **135**, 373 (1983).
8. S. Fujikawa and T. Akamatsu, *ibid.* **97**, 481 (1980).
9. J. N. Israelachvili and G. E. Adams, *J. Chem. Soc. Faraday Trans. 1* **74**, 975 (1978).
10. J. Israelachvili, *Nature Phys. Sci.* **229**, 85 (1971); *J. Colloid Interface Sci.* **44**, 259 (1973).
11. C. A. Helm, J. N. Israelachvili, P. M. McGuiggan, *Science* **246**, 919 (1989).
12. R. G. Horn, J. N. Israelachvili, F. Pribac, *J. Colloid Interface Sci.* **115**, 480 (1987).
13. H. K. Christenson and P. M. Claesson, *Science* **239**, 390 (1988).
14. L. R. Fisher and J. N. Israelachvili, *Colloids Surfaces* **3**, 303 (1981); H. K. Christenson, *J. Colloid Interface Sci.* **104**, 234 (1985).
15. R. H. Colby, L. J. Fetters, W. W. Graessly, *Macromolecules* **20**, 2226 (1987).
16. R. Gohar, *Elastohydrodynamics* (Horwood, Chichester, UK, 1988); D. Dowson and G. R. Higginson, *Elastohydrodynamic Lubrication* (Pergamon, Oxford, 1977).
17. J. N. Israelachvili and S. J. Kott, *J. Chem. Phys.* **88**, 7162 (1988).
18. J. C. Fisher, *J. Appl. Phys.* **19**, 1062 (1948).
19. Y. L. Chen and J. N. Israelachvili, in preparation.
20. D. Dowson and C. M. Taylor, *Annu. Rev. Fluid Mech.* **11**, 35 (1979).
21. H. W. Strube and W. Lauterborn, *Z. Angew. Phys.* **29**, 349 (1970).
22. We thank C. Brennan, D. Dowson, A. T. Ellis, F. Lang, W. Lauterborn, G. Leal, A. Prosperetti, R. Simoneau, and M. P. Tullin for comments and L. J. Fetters of Exxon Research Laboratories for providing the PBD liquids. This work was supported under Office of Naval Research grant N00014-89-J-1101.

27 November 1990; accepted 8 March 1991

The Chemical Nature of Buckminsterfullerene (C_{60}) and the Characterization of a Platinum Derivative

PAUL J. FAGAN,* JOSEPH C. CALABRESE, BRIAN MALONE

Little is known about the chemical nature of the recently isolated carbon clusters (C_{60}, C_{70}, C_{84}, and so forth). One potential application of these materials is as highly dispersed supports for metal catalysts, and therefore the question of how metal atoms bind to C_{60} is of interest. Reaction of C_{60} with organometallic ruthenium and platinum reagents has shown that metals can be attached directly to the carbon framework. The native geometry of C_{60} is almost ideally constructed for dihapto-bonding to a transition metal, and an x-ray diffraction analysis of the platinum complex $[(C_6H_5)_3P]_2Pt(\eta^2\text{-}C_{60})\cdot C_4H_8O$ revealed a structure similar to that known for $[(C_6H_5)_3P]_2Pt(\eta^2\text{-ethylene})$. The reactivity of C_{60} is not like that of relatively electron-rich planar aromatic molecules such as benzene. The carbon-carbon double bonds of C_{60} react like those of very electron-deficient arenes and alkenes.

THE PROPERTIES OF THE RECENTLY isolated carbon clusters (*1*) have attracted considerable attention with regard to theoretical and physical properties (*2–4*), but there are few reports concerning the chemistry of these species (*3–4*). One well-defined derivative has been reported, namely, the osmium tetroxide adduct structurally characterized by Hawkins *et al.* (*3*). We investigated organometallic derivatives of C_{60} to ascertain its chemical nature and report the reactions of C_{60} with the reagents $[(C_6H_5)_3P]_2Pt(\eta^2\text{-}C_2H_4)$ (*5*) and $[Cp^*Ru(CH_3CN)_3]^+O_3SCF_3^-$ [$Cp^* = \eta^5\text{-}C_5(CH_3)_5$] (*6*). Zero-valent Pt compounds are well known to react with electron-poor alkenes and arenes bonding in a dihapto-fashion, but are unreactive toward relatively electron-rich aromatic molecules such as benzene (*5*). In contrast, when $[Cp^*Ru(CH_3CN)_3]^+O_3SCF_3^-$ is reacted with relatively electron-rich planar arenes, the three coordinated acetonitriles are displaced resulting in strong, hexahapto-binding of ruthenium to the six-membered ring of the arene (*6*).

Addition of $[(C_6H_5)_3P]_2Pt(\eta^2\text{-}C_2H_4)$ (31 mg) to C_{60} (30 mg) in toluene (2 ml) under a dinitrogen atmosphere resulted in formation of an emerald-green solution from which black microcrystals precipitated over the course of 2 hours. This precipitate was collected by filtration, washed twice with 2-ml portions of toluene and then with 10 ml of hexane, and dried by pulling N_2 through the filter cake. It was recrystallized by first dissolving in tetrahydrofuran (THF), filtering, concentrating, and precipitating with hexane. The isolated yield of this compound was 85% based on the formulation $[(C_6H_5)_3P]_2Pt(\eta^2\text{-}C_{60})$ (THF of crystallization is removed upon drying under vacuum). Elemental analytical data supported this formulation (*7*). The ^{31}P nuclear magnetic resonance (NMR) spectrum (121.7 MHz, external standard H_3PO_4) of this compound in THF-d_8 displayed a singlet at δ 27.0 ppm with satellites due to coupling of ^{31}P to the spin-1/2 isotope ^{195}Pt (33.8 % abundance) ($J_{P\text{-}Pt}$ = 3936 Hz). For comparison, the shift observed for $[(C_6H_5)_3P]_2Pt(\eta^2\text{-}C_2H_4)$ is δ 34.8 with a coupling constant $J_{P\text{-}Pt}$ = 3738 Hz. Since these coupling constants and chemical shifts were similar, it suggested that the coordination sphere about Pt was nearly identical in both the ethylene and C_{60} complexes.

In order to substantiate this proposal, we performed a single-crystal x-ray structural analysis of the complex $[(C_6H_5)_3P]_2Pt(\eta^2\text{-}C_{60})\cdot C_4H_8O$. Small multiple needles were grown by slow evaporation from THF. A thin needle was cut in half to obtain a weakly diffracting single crystal from which x-ray data were successfully collected and analyzed (*8*). Accuracy of the structure was limited because of the small size of the crystal and disorder associated with THF molecules contained in the lattice (Fig. 1). The bonding parameters within the C_{60} framework agree closely with those obtained for the osmium tetroxide derivative of Hawkins *et al.* (*3*). In this case, Pt serves to anchor the molecule and reduce disorder problems. Rotation of alkenes about the platinum-alkene bond has a substantial energy barrier (*9*). The bis(triphenylphosphine)platinum moiety bonds to two carbon atoms of the C_{60} molecule at the junction of two fused six-membered rings rather than at the junction of the five- and six-membered rings. The bonding pattern is reminiscent of other structurally characterized transition metal–alkene complexes (*9, 10*). Bond distances and bond angles about Pt are shown in Fig. 2. The metrical data agree with those previously established for $[(C_6H_5)_3P]_2Pt(\eta^2\text{-}C_2H_4)$ (*10*).

It is well known that upon coordination of a transition metal such as Pt to an alkene, the four groups attached to the carbon-carbon double bond splay back away from the metal center (*11*). One measure of this distortion is to determine the degree to which two groups attached to one end of a double bond bend back relative to remaining planar. This can be defined as the angle between the vector described by the two doubly bonded carbons and the plane defined by one of these carbons and the two groups attached to it. Typical angles in Pt complexes with unconstrained carbon-substituted alkenes range from approximately 22° to 35° (*12*). In this regard, the natural curvature of C_{60} should permit bonding to a

Central Research and Development Department, E. I. du Pont de Nemours & Co., Inc., Experimental Station, Wilmington, DE 19880–0328.

*To whom correspondence should be addressed.